

Prevention of pressure oscillations in modeling a cavitated acoustic fluid

Bradley Klenow and Dr. Alan Brown
Department of Aerospace and Ocean Engineering
Virginia Polytechnic Institute and State University
Blacksburg, VA 24061

Cavitation effects play an important role in the UNDEX loading of a structure. For far-field UNDEX, the structural loading is affected by formation of local and bulk cavitation regions, and a pressure pulse resulting from the closure of the cavitation region. A common approach to numerically modeling cavitation in far-field underwater explosions is using Cavitating Acoustic Finite Elements (CAFE) and more recently Cavitating Acoustic Spectral Elements (CASE). Treatment of cavitation in this manner causes spurious pressure oscillations which must be treated by a numerical damping scheme. The focus of this paper is to investigate a new method, based on the original Boris and Book Flux-Corrected Transport algorithm [1], to limit oscillations without the energy loss associated with the current damping scheme.

Introduction and Background

For the past 20 years the finite element method (FEM) has been frequently used to model far-field underwater explosion (UNDEX) phenomena. A far-field underwater explosion is defined here as an UNDEX where the charge is located a significant distance away from the structure such that effects from the explosive gas bubble are negligible and any structural deformation is elastic. Far-field underwater explosions are of practical interest because they are the type of UNDEX used in Navy ship shock trials (see e.g., [2]). The ultimate goal of applying FEM to far-field UNDEX problems is to accurately simulate full scale ship shock trials to aid in the design of new naval ships.

A FE model of far-field UNDEX generally consists of a structure domain, a modeled fluid domain, and a fluid boundary which is treated as a non-reflecting boundary. The fluid model must treat three UNDEX phenomena: the incident shock wave, cavitation, and the resulting fluid-structure interaction. The incident shock wave is a step exponential wave that results from the explosion. It is important to note that a far-field FE model does not include the charge. Instead the incident shock wave is initialized inside the fluid mesh via the initial conditions. Cavitation results from the pressure in the surrounding water dropping below its vapor pressure due to the displacement of the ship structure (local cavitation) or the tensile shock wave reflected from the free surface (bulk cavitation).

Both the incident shock wave and the cavitation region present computational difficulties in far-field UNDEX finite element models. The incident shock wave is a discontinuous wave, making distortion of the wave front and loss of pressure magnitude a concern. Cavitation creates a material discontinuity in the fluid and causes a secondary shock loading upon closure. The formation of the cavitation region is also affected by dissipation of the reflected shock wave. Distortion and dissipation of the incident, reflected, and cavitation closure shock waves as well as the discontinuous nature of cavitation create the need for FE models of far-field UNDEX to have highly refined meshes for accurate solutions.

The need for a highly refined mesh in far-field UNDEX FE models is a major obstacle in the ability to accurately simulate ship shock trials because a far-field UNDEX model requires a substantial amount of fluid to be modeled, especially in a full scale three-dimensional problem. In these types of problems the size requirement of the fluid model coupled with the refinement cause the computational effort to be extreme.

The size requirements of the fluid domain and the far-field fluid/structural assumptions have made treating the fluid as an acoustic fluid with scalar unknowns a popular choice in far-field UNDEX FE models. An acoustic fluid is one in which disturbances in the fluid propagate rapidly and are linearizable, even if the constitutive behavior (i.e., cavitation phenomena) of the fluid is non-linear [3]. Such a treatment is valid in the far-field problem, because shock and cavitation loading are early time events, occurring on the order of micro-seconds. Because of the short time duration of these events, the ship as whole does not exhibit a global response to the loading. Furthermore the effects of the gas bubble and hull rupture, two phenomena that cause large fluid displacements, are neglected. Thus the far-field problem is of short duration and the global fluid displacement is small, which satisfy conditions for acoustic treatment given in [4].

Cavitating Acoustic Finite Elements

Newton [5,6] developed one of the first FEM cavitation models using the displacement potential formulation of the acoustic wave equation. In his cavitation model a bilinear constitutive equation is used to treat the cavitation region as a homogenous single phase region of constant total pressure equal to the vapor pressure of water. In most models the vapor pressure of water is taken to be 0 Pa because the large difference between the magnitude of vapor pressure, $\sim 10^3$ Pa, and hydrostatic pressure, $\sim 10^5$ Pa, negates any effect of using the actual vapor pressure in the cavitation region.

This type of cavitation model is a one-fluid, cut-off cavitation model. One-fluid refers to the single governing equation used to model two separate phases of the fluid. The advantage of a one-fluid model is computational savings, especially in large scale problems, over a two-fluid model which requires multiple fluid equations to be solved.

Cut-off refers to the method by which the cavitation model forces the total pressure of the fluid to be the vapor pressure of water once the cavitation criteria is met. The disadvantage of cut-off treatment is that the phase transition between water and vapor is not explicitly considered. However, in large scale problems, such as a far-field UNDEX, cut-off models have performed almost identically to cavitation models that include phase transition [7,8]

Newton's cavitation model was used by Zienkiewicz, Paul, and Hinton [9] to study cavitation effects on dam loading. In their model an unconditionally stable implicit time integration scheme was introduced, with an iterative check for cavitation. Felippa and DeRuntz [3,10] latter used Newton's cavitation model in the development of the Cavitating Fluid Analyzer (CFA) code. The CFA code extended Newton's model to three dimensions, incorporated a conditionally stable staggered central difference time integration scheme, a node-by-node (non-iterative) check for cavitation, and coupled the fluid boundary to the boundary element code USA to act as a non-reflecting boundary. This approach has been incorporated into the commercial FEM code LS-DYNA [11] and has been used by many researchers in far-field UNDEX modeling applications [2,11-14]. The common name for the approach created by Felippa and DeRuntz is the cavitating acoustic finite element (CAFE) approach.

There are several aspects of the CAFE approach that limit its effectiveness, especially for large scale problems. The first deficiency in the CAFE approach is the use of linear (1D), bi-linear (2D), or tri-linear (3D) elements in the fluid mesh. Because low order elements are used, CAFE fluid meshes are highly dispersive [15,16]. This makes the CAFE approach highly susceptible to the mesh refinement needs discussed in the previous section. Such a high level of CAFE mesh refinement is often not feasible for full ship far-field UNDEX models.

Another deficiency of the CAFE approach is that one-to-one nodal coupling is required at every point on the fluid structure interface. The one-to-one coupling requirement makes it extremely difficult to couple a complex structure to the fluid. In addition to this, one-to-one coupling requires that any mesh refinement in the fluid must also be carried out on the structural elements on the fluid-structure interface [16]. Such structural refinements are not necessary and cause an increase in the critical time step of the model because of the difference in material sound speed (with most solids being much greater than water).

Cavitating Acoustic Spectral Elements

To address the highly dispersive nature of the CAFE approach Sprague and Geers employed higher order spectral elements (SE) to discretize the governing CAFE equations [15-17]. They called their new approach Cavitating Acoustic Spectral Elements (CASE).

Spectral elements are a combination of spectral methods and FEM. Spectral methods use high order basis functions derived from orthogonal polynomials to reduce interpolation error at the integration points or nodes. Typically either Chebyshev or Legendre polynomials are used for the orthogonal polynomials that make up the basis functions in the spectral element method (SEM). Sprague and Geers preferred Legendre polynomials because of their superior performance in wave propagation problems [16] and used Gauss-Lobatto-Legendre (GLL) quadrature for the node/interpolation points.

These high order spectral basis functions are generally less dispersive than low order basis functions and can exhibit exponential convergence for problems with smooth solutions [18]. When combined with FEM, the spectral basis functions are applied to each element using a sub-parametric mapping, rather than the entire domain. The result is a method that retains the geometric flexibility of FEM and the high order accuracy of spectral methods [16].

The application of spectral elements in the CASE approach improves the dispersion and super refinement issues encountered in the CAFE approach. The result is a savings in required degrees of freedom, which in turn reduces total operations and memory storage. Sprague and Geers also incorporated a constant-interpolation coupling [19] algorithm to couple the fluid to the structure and field separation. The coupling algorithm removes the need for one-to-one nodal coupling along the fluid-structure interface, making coupling complex structures to the fluid easier and also allowing the fluid mesh to be refined separately from the structural mesh [16].

Another addition to the CASE approach used by Sprague and Geers was field separation. Field separation separates the fluid into a known incident field (the incident shock wave) and the unknown scattered field (the reflected shock and cavitation region) which are combined, via superposition, to obtain the total field. The advantage of field separation is that the incident shock wave can be propagated through the mesh without being distorted.

Despite the advantages of the CASE approach there are deficiencies that limit its effectiveness in certain problems. One disadvantage is that spectral elements produce larger maximum mesh eigenvalues and therefore require smaller critical time steps for explicit time integration. An important implication of the reduced critical time step is that when compared to a CAFE model with the same number of total degrees of freedom a CASE model is more computationally expensive.

The most significant disadvantage of the CASE approach is the tendency of spectral elements to increase spurious oscillations in problems with discontinuities. Spurious oscillations due to cavitation formation in the CAFE approach were initially discussed by Newton [5]. Newton observed that isolated regions of cavitation fluid can appear within the pressurized fluid. He termed this phenomena “frothing”. We have observed that frothing occurs in the pressurized fluid that exists between the upper cavitation boundary and the structure/free surface. The absence of frothing does not mean oscillations have been sufficiently damped, only that the magnitude of the oscillations has not reached the cavitation cut-off condition. These oscillations are unique to cavitation problems because they form from a combination of discontinuous wave propagation (the reflected wave front), a material discontinuity in the fluid (cavitation region boundaries), and the application of the cavitation model itself. Spurious cavitation oscillations are worse in the CASE approach than in CAFE because spectral methods incur larger Gibbs phenomenon errors [20] in regions of discontinuity such as the discontinuous wave and the material discontinuity in a cavitation region.

Sprague and Geers used [21] and [22] to argue that information pertinent to the solution are contained in these oscillations, and are therefore acceptable. Giannakouros and Karniadakis [22] explain that despite large amplitude oscillations in the domain, the propagating discontinuity moves at the correct speed. They showed this implied information is contained in the oscillations and therefore, spectral schemes must retain more information. This holds true for oscillations that arise from shock wave propagation, which we have found are well smoothed by the artificial damping scheme used in CASE. However, spurious oscillations that result from formation of the cavitation region are different in nature from oscillations that arise from shock propagation. Furthermore, cavitation oscillations are often much more problematic than spurious oscillations that result from discontinuous wave propagation and are not well smoothed by the CASE damping scheme. Therefore, we believe while information may be contained in spurious cavitation oscillations, their presence degrades the accuracy of model because they have a much larger affect than oscillations that arise from shock propagation.

An Overview of Flux-Corrected Transport

Given the advantages and disadvantages of both the CAFE and CASE approaches we seek a new approach that combines the less diffusive nature of CASE with the less oscillatory nature and reduced computational expense of CAFE. To accomplish this we use a finite element flux-corrected transport (FE-FCT) method proposed by Xiao [23] for structured grids. The flux-corrected transport method was developed by Boris and Book [1,24,25] to predict smooth finite difference solutions to one-dimensional shock problems in compressible fluids governed by the continuity and/or Euler equations. In general a flux corrected transport algorithm consists of a transported diffusion stage and an anti-diffusion stage. The transported diffusion stage advances the solution in time and gives a smooth or diffused solution. The anti-diffusion stage seeks to correct the numerical errors introduced by the diffused solution by correcting or limiting the anti-diffusive fluxes. Flux correction or limitation allows anti-diffusion to be

implemented without allowing existing oscillations to grow or causing new oscillations [1], thus it is a crucial part of the FCT method.

Zalesak [26,27] extended flux limitation and FCT to a general multidimensional form by using the combination of a high and low order numerical scheme. The low order scheme, like the diffusion stage of the original algorithm, gives a smooth solution in regions of discontinuity. The high order scheme gives a more accurate solution in smooth regions of the solution. The FCT algorithm developed by Zalesak has been applied to many problems involving shocks in fluids. Similar FCT algorithms have been developed FEM [28,29] and even SEM [20,22].

For far-field UNDEX problems the FE-FCT algorithm introduced by Xiao is ideal because it does not require the combination of a high and low order scheme. Use of a high and low order scheme would be too computationally expensive for full scale far-field UNDEX problems. FE-FCT is a well suited method for application to CAFE like methods because it both smoothes the solution, which is needed to capture cavitation, and restores accuracy, which is need to capture the initial and reflected shock wave. Another beneficial attribute of FE-FCT algorithms for UNDEX applications is that they are typically less diffusive than artificial damping schemes. This is important for CAFE/CASE methods because the amount of artificial damping needed to adequately smooth cavitation oscillations often over damps the energy associated with shock wave propagation.

Xiao's FE-FCT Algorithm

A general representation of the FCT algorithm devised by Boris and Book [1] for finite difference methods and extended to the finite element method by Xiao [23] is given below. Following Xiao's routine, let ψ be a function of time and space in one-dimension. The value of ψ at time step $n+1$ and location x (represented by nodal index j) is written as,

$$\psi_j^{n+1} = f(\psi_j^n, \Delta t, \Delta h), \quad (1)$$

a function of the value of ψ_j at time step n , time step Δt , and element length Δh . Xiao's FE-FCT algorithm consists of the following steps:

Algorithm 1 [23]:

1. Compute transported solution. In Xiao's FE-FCT method the transported solution is obtained by the trial values of ψ_j at time step $n+1$:

$$\tilde{\psi}_j^{n+1} = f(\psi_j^n, \Delta t, \Delta h). \quad (2)$$

2. Compute the diffusive fluxes:

$$\varphi_j^D = \eta_D(\psi_{j+1}^n - \psi_j^n), \quad (3)$$

where η_D is the diffusion coefficient.

3. Compute the transported diffused solution:

4.

$$\psi_j^{TD} = \tilde{\psi}_j^{n+1} + \varphi_j^D - \varphi_{j-1}^D. \quad (4)$$

5. Compute the anti-diffusive fluxes:

$$\varphi_j^A = \eta_A(\tilde{\psi}_{j+1}^n - \tilde{\psi}_j^n), \quad (5)$$

where η_A is the anti-diffusion coefficient.

6. Limit/correct the anti-diffusive fluxes:

7.

$$\varphi_j^C = S \cdot \max\{0, \min(S \cdot \Delta_{j-1}, |\varphi_j^A|, S \cdot \Delta_{j+1})\}, \quad (6)$$

where $\Delta_{j\pm 1} = \pm(\psi_{j\pm 1}^{TD} - \psi_j^{TD})$ and $S = \text{sign}(\varphi_j^A)$.

8. Apply the corrected anti-diffusive fluxes to the solution:

9.

$$\psi_j^{n+1} = \psi_j^{TD} + \varphi_j^C - \varphi_{j-1}^C. \quad (7)$$

To apply Xiao's FE-FCT algorithm to a CAFE/CASE far-field UNDEX model, we must slightly modify our approach to modeling the fluid. CAFE and CASE are both governed by the displacement potential form of the acoustic wave equation (AWE). In this form the governing equation for a cavitating fluid is expressed as a relation

between condensation (volumetric strain) and the Laplacian of displacement potential. The pressure form of the AWE for a cavitating fluid, which is a relation between the second time derivative of pressure and the Laplacian of pressure, is better suited for Xiao's FE-FCT method because it retains the time derivative term in the AWE. Thus we apply Xiao's FE-FCT method to the pressure form of the AWE rather than the displacement potential used in the CAFE/CASE approach.

Governing Fluid Equations

The pressure form of the AWE is obtained by first assuming that the reference density of the fluid, ρ_o , is constant and that fluctuations between the density, ρ , and ρ_o remain small. This allows the continuity equation with velocity field \vec{u} ,

$$\frac{\partial \rho}{\partial t} + \nabla \cdot (\rho \vec{u}) = 0, \quad (8)$$

to be written in terms of condensation, ($s = \frac{\rho}{\rho_o} - 1$),

$$\frac{\partial s}{\partial t} + \nabla \cdot (\vec{u}) = 0, \quad (9)$$

for $|s| \ll 1$. If we neglect body forces, viscosity, and convective acceleration terms, then conservation of momentum for the acoustic fluid becomes Euler's equation

$$\rho_o \frac{\partial \vec{u}}{\partial t} + \nabla p = 0, \quad (10)$$

where p is the dynamic pressure. By taking the first time derivative of eq. (9) and the divergence of eq. (10) we obtain two new equations that when related to each other the term, $\nabla \cdot \left(\frac{\partial \vec{u}}{\partial t}\right)$, can be canceled between them. This procedure yields the relation

$$\frac{1}{c^2} \frac{\partial^2 s}{\partial t^2} + \nabla^2 p = 0, \quad (11)$$

where c is the speed of sound in the acoustic fluid. Using an adiabatic equation of state for the acoustic fluid (see e.g., [30]),

$$p = \rho c^2 s, \quad (12)$$

we obtain the pressure form of the acoustic wave equation

$$\frac{1}{c^2} \frac{\partial^2 p}{\partial t^2} + \nabla^2 p = 0. \quad (14)$$

In 2001 Nimmagadda and Cipolla [31] derived a cavitation model for eq. (14). This cavitation model coupled with the pressure form of the AWE are used in the commercial finite element code ABAQUS [32]. Nimmagadda and Cipolla defined a "pseudo pressure" as the material state variable instead of condensation (as in CAFE/CASE). Following their approach, the pseudo pressure is given by

$$p_v = -\rho c^2 (\nabla \cdot \vec{\xi}), \quad (15)$$

where $\vec{\xi}$ is the fluid displacement field. Following a similar procedure to that used to obtain eq. (11) the cavitating form of eq. (14) becomes

$$\frac{1}{c^2} \frac{\partial^2 p_v}{\partial t^2} + \nabla^2 p = 0. \quad (16)$$

The equation of state for p is now determined by the cavitation model

$$p = \max(-p_h, p_v), \quad (17)$$

where p_h is the hydrostatic pressure. Note that the cavitation model in eq. (17) is a one-fluid cut-off model that satisfies the condition that the total pressure ($p_t = p + p_h$) in the cavitation region is zero.

Finite Element Formulation

We discretize the governing fluid equation eq. (16) using the Galerkin approach. Pre-multiplying eq. (16) by test function ϕ and integrating over the fluid domain Ω gives

$$\int_{\Omega} \left[\frac{1}{c^2} \frac{\partial^2 p_v}{\partial t^2} \phi + \nabla^2 p \phi \right] d\Omega = 0. \quad (18)$$

Applying Green's first identity to eq. (18) yields the weak form of the governing equation

$$\frac{1}{c^2} \int_{\Omega} \ddot{p}_v \phi \, d\Omega - \int_{\Omega} \nabla p \cdot \nabla \phi \, d\Omega = \int_{\Gamma} \phi \nabla p \cdot \vec{n} \, d\Gamma, \quad (19)$$

where Γ denotes the fluid boundary in domain Ω and \vec{n} is the outward pointing normal vector on Γ . We approximate the pseudo pressure, dynamic pressure, and test function in eq. (19) using piecewise linear basis functions, which gives the matrix equation

$$\mathbf{Q}\ddot{\mathbf{p}}_v + \mathbf{H}\mathbf{p} = \mathbf{b}, \quad (20)$$

where \mathbf{Q} is the capacitance matrix, \mathbf{H} is the reactance matrix, and \mathbf{b} is the fluid force vector. The integrals in eq. (19) are found using Gauss-Lobatto-Legendre quadrature. A critical aspect of Xiao's FE-FCT scheme is that the algorithm corrects each corrected variable separately. This implies that each corrected variable must be independent, which makes the FE-FCT scheme explicit. Therefore, the capacitance matrix \mathbf{Q} must be lumped. This is done using the row-sum technique.

Boundary Conditions

For far-field UNDEX there are three main types of boundaries that are applied to eq. (19): known pressure, fluid-structure interaction, and non-reflecting boundaries (NRBC). Known pressure boundaries are boundaries where p is known for all time. A key known pressure boundary for far-field UNDEX is the fluid free surface boundary condition [4]

$$p = 0. \quad (21)$$

On fluid-structure interaction boundaries we assume that the fluid and structure have the same displacements and for now we also take the fluid and structure nodes on the fluid-structure boundary to be coincident. Recall that this is the approach taken in the original CAFE method. The fluid-structure interaction boundary condition for eq. (19) is

$$\vec{n}_s \cdot \vec{a}_s = -\frac{1}{\rho_o} \frac{\partial p}{\partial n}, \quad (22)$$

where \vec{n}_s is the normal vector on the fluid-structure boundary pointing into the fluid in direction n and \vec{a}_s is the structural acceleration field on the fluid-structure boundary. This boundary condition is used to determine the fluid force vector \mathbf{b} .

Non-reflecting boundaries allow the modeled fluid domain, which is finite, to be treated numerically as an infinite domain [33]. Such treatment is necessary for far-field UNDEX problems because physically the fluid region it is part of a large body of water [34]. For this work we apply the Somerfeld NRBC [33] given in eq. (23), which is exact for one-dimensional plane waves.

$$\frac{\partial p}{\partial n} = -\frac{1}{c} \frac{\partial p}{\partial t}. \quad (23)$$

Application of eq. (23) to eq. (19) yields a new matrix equation

$$\mathbf{Q}\ddot{\mathbf{p}}_v + \mathbf{D}\dot{\mathbf{p}}_v + \mathbf{H}\mathbf{p} = \mathbf{b}, \quad (24)$$

where \mathbf{D} is a diagonal "damping" matrix that has non-zero terms, $-\frac{1}{c}$, only on NRBC boundary nodes [33]. While the Somerfeld NRBC, eq. (23), is easy to implement and works well in one-dimension, more complex NRBCs are required for accurate solutions to more realistic UNDEX problems. Sprague and Geers used the curved wave approximation [16] which is also implemented in ABAQUS [32]. Felippa and DeRuntz used the doubly asymptotic approximation (DAA) [10,35] for the CAFE method. The DAA allows for the added mass effects of the infinite fluid to be accounted for.

Application of FE-FCT Algorithm to the Acoustic Wave Equation

We now apply Xiao's FE-FCT algorithm to the cavitating acoustic formulation given in discretized form by eqs. (19) and (24) and subject to the boundary conditions described above. Following [23], we begin by re-writing eq. (24) as the following differential equation

$$\frac{\partial \dot{p}_{v,i}}{\partial t} = \frac{f_i^{ext} - f_i^{int}}{M_{ii}}, \quad (25)$$

where i is a nodal index. Note the following application is for a one-dimensional problem but it can also be applied to a multidimensional problem where the discontinuous wave is a plane wave. In this case $\dot{p}_{v,i}$ would be corrected in the direction of wave propagation only. Further extension of this algorithm to multiple dimensions for general cases is provided in [23] and [36].

In the following equations n is the time step number and i is a nodal index:

Algorithm 2:

1. Compute the nodal forces:

$$f^{ext} = \mathbf{b}, \quad (26)$$

$$f^{int} = \mathbf{H}p^n - \mathbf{D}\dot{p}_v^n. \quad (27)$$

2. Compute the trial \dot{p}_v :

$$\tilde{p}_i^{n+1} = \dot{p}_{v,i}^n + \left(\frac{f_i^{ext} - f_i^{int}}{M_{ii}} \right) \Delta t. \quad (28)$$

3. Compute the diffusive fluxes:

$$\varphi_i^D = \eta_D (\dot{p}_{v,i+1}^n - \dot{p}_{v,i}^n), \quad (29)$$

4. Compute the transported diffused solution:

$$\dot{p}_{v,i}^{TD} = \tilde{p}_{v,i}^{n+1} + \varphi_i^D - \varphi_{i-1}^D. \quad (30)$$

5. Compute the anti-diffusive fluxes:

$$\varphi_i^A = \eta_A (\tilde{p}_{v,i+1}^n - \tilde{p}_{v,i}^n), \quad (31)$$

6. Limit/correct the anti-diffusive fluxes:

$$\varphi_i^C = S \cdot \max\{0, \min(S \cdot \Delta_{i-1}, |\varphi_i^A|, S \cdot \Delta_{i+1})\}, \quad (32)$$

where $\Delta_{i\pm 1} = \pm(\dot{p}_{v,i\pm 1}^{TD} - \dot{p}_{v,i}^{TD})$ and $S = \text{sign}(\varphi_i^A)$.

7. Apply the corrected anti-diffusive fluxes to the solution:

$$\dot{p}_{v,i}^{n+1} = \dot{p}_{v,i}^{TD} + \varphi_i^C - \varphi_{i-1}^C. \quad (33)$$

8. Update pseudo pressure (eq. (34)) and check for cavitation using eq. (17) on each node:

$$p_v^{n+1} = p_v^n + \Delta t \dot{p}_v^{n+1}. \quad (34)$$

9. Apply known pressure boundary conditions and advance to next time step.

The diffusive, η_D , and anti-diffusive, η_A , coefficients are constants, chosen to suit a particular problem or algorithm. Boris and Book gave $\eta_D = \eta_A = 1/8$ [1,25] as the optimal choice of coefficients for Algorithm 2. These same coefficients were also used by Xiao. While there are no strict rules for choosing the coefficients, in general, $\eta_D \geq \eta_A$, to prevent the growth of new oscillations in the anti-diffusion stage. For the anti-diffusion stage to fully correct the errors introduced in the diffusion stage, $\eta_D \equiv \eta_A$. This last requirement is problematic for cavitation problems. In order to ensure a smooth solution after the anti-diffusion stage, the diffusion stage must remove all oscillations [27]. Because spurious oscillations are inherent to our cavitation scheme, we cannot ensure that the

diffusion stage adequately smoothes the solution. Therefore, for a cavitation problem the solution will retain oscillations after the anti-diffusion stage as the flux limiter. Equation (32) no longer guarantees the formation of new oscillations or the non-growth of existing oscillations.

A solution to this problem is to not fully correct the solution in the anti-diffusion stage by taking, $\eta_D \geq \eta_A$. The effect of this is to over diffuse the solution to smooth cavitation oscillations, as in the CAFE/CASE method. By adding some anti-diffusion to the solution we hope to remove most of the effect of over diffusion on accuracy but not its effect on oscillations. In taking this approach in applying the FE-FCT algorithm to cavitation problems we have found that the existing flux limiter eq. (32) tends to over damp the solution even after the anti-diffusion stage. The explanation for this is that the limiter in eq. (32), which is termed a strong flux limiter [1], tends to over correct the anti-diffusive fluxes in some areas. One key area is in regions of sharp peaks such as the hypothetical solution shown in Fig. 1. In these regions strong flux limitation tends to remove the peak and replace it with a terraced region, as illustrated in Fig. 1. This phenomenon is called clipping [24,26]. To overcome clipping and the over diffusive nature of strong flux limiting for $\eta_D > \eta_A$, we have adapted a double one-sided flux limiter [24], given by eq. (35), to Xiao's FE-FCT algorithm.

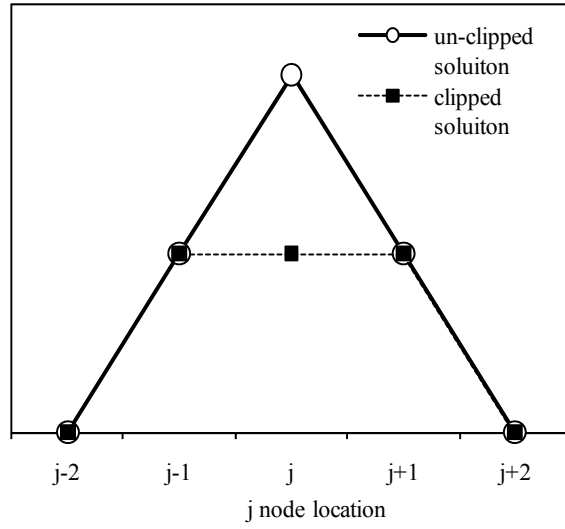


Figure 1. Illustration of a hypothetical solution that has been "clipped" after application of strong flux limitation (eq.(6))

$$\varphi_i^C = S \cdot \max\{0, \min(S \cdot \Delta_{i'}, |\varphi_i^A|)\}, \quad (35)$$

where,

$$\Delta_{i'} = \begin{cases} \dot{p}_{v,i}^{TD} - \dot{p}_{v,i-1}^{TD}, \dots \text{ if } S \cdot \dot{p}_{v,i}^n \geq 0 \\ \dot{p}_{v,i+1}^{TD} - \dot{p}_{v,i}^{TD}, \dots \text{ if } S \cdot \dot{p}_{v,i}^n < 0 \end{cases}$$

Compared to strong flux limitation double sided flux limitation (eq. (35)) allows more oscillations, however eq. (35) allows calculation of the solution regions of greatest variance to 0 (e.g. shock waves and cavitation regions) with high accuracy [24]. This is a key feature for cavitation problems because we have decided to treat cavitation oscillations by over diffusing the solution. Therefore, we require the anti-diffusion stage to be as accurate as possible in regions away from cavitation oscillations where we have large amplitude peaks such as shock fronts and cavitation boundaries to mitigate the effect of over diffusion.

Example Problem

To evaluate the effectiveness of the FE-FCT algorithm when applied to a far-field UNDEX problem we use a two degree of freedom mass-spring oscillator problem shown in Fig. 2. The problem consists of a structure consisting of masses m_1 and m_2 , with displacements $d_1(t)$ and $d_2(t)$, sitting on top a column of fluid with depth L . The masses are connected by a spring with spring constant k and are initially at rest. At time $t=0$ the wave front of the incident shock wave, modeled as a plane step exponential wave, is located at x_{SO} .

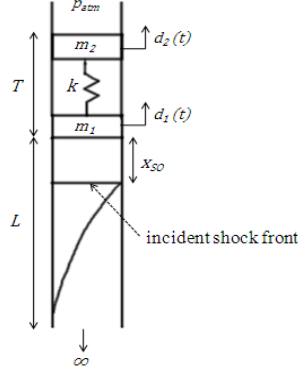


Figure 2. Schematic of the mass-spring oscillator UNDEX problem

This problem was originally solved by Sprague and Geers in [37] using the CAFE approach and latter using the CASE approach [17]. Solutions using the approach of Nimmagadda and Cipolla are given in the ABAQUS manual [38] and most recently the problem has been solved in [39] using a ghost fluid method with an Eulerian fluid.

We solve this problem for the $m_1/m_2 = 5$ case in one-dimension using the CASE model in [17] and by applying our own FE-FCT method in one-dimension. Note the masses are modeled as lumped mass elements and the infinite boundary treated with the Somerfeld NRBC eq. (23).

For this evaluation we wish to examine the effectiveness of the FE-FCT algorithm to both accurately capture cavitation phenomena and reduce cavitation oscillations. Therefore we use the scattered field formulation (SFM) of Sprague and Geers [17]. This allows comparison of CAFE, CASE, and FE-FCT in terms of capturing cavitation phenomena only, avoiding errors associated with propagating the incident shock wave through the fluid model. Using SFM for our formulation requires the total pressure and pseudo pressure to be written as

$$p_t = p_l + p_s + p_h, \quad (38)$$

$$p_{v,t} = p_{v,l} + p_{v,s}, \quad (37)$$

where p_s , $p_{v,s}$, p_l , and $p_{v,l}$ are the scattered pressure, scattered pseudo pressure, incident pressure, and incident pseudo pressure respectively. The incident pressure (i.e. the shock wave) in this problem is given as

$$p_l(x, t) = P_{peak} \exp \left[-\frac{t + (x - x_{SO})/c}{\tau} \right] \mathcal{H}(t + (x - x_{SO})/c), \quad (38)$$

where $\mathcal{H}(t)$ is the heaviside function, P_{peak} is the peak pressure of the shock wave and τ is the decay constant. For acoustic UNDEX models this pressure is taken as the pressure given by the peak approximation [40,41] at the fluid structure interface. The decay constant, τ , for the shock wave is found by a similar empirical equation [41]. Also note that for SFM the fluid forcing term given by the boundary condition in eq. (22) becomes (in one-dimension)

$$\ddot{d}_{s,1} = -\frac{1}{\rho_o} \frac{\partial p}{\partial x}, \quad (39)$$

where $\ddot{d}_{s,1}$ is now the scattered acceleration of mass m_1 . The fluid and structure are coupled together using a staggered solution procedure similar to the one used in [10] for the CAFE method. The mass-spring system is integrated in time with the central difference method.

For the Sprague and Geers problem in [17] the fluid has depth $L = 3.0$ m and we take $\rho_o = 1025$ kg/m³, $c = 1450$ m/s, and $p_{atm} = 101.3$ kPa. The structure has a draft, $T = 5.08$ m, a total mass, $m_1 + m_2 = 5270$ kg, and $k = (10\pi)^2 m_2$. The peak pressure is $P_{peak} = 16.12$ MPa, the decay constant is $\tau = 0.423$ ms, and $x_{SO} = 0$ m. The incident shock wave used is the equivalent to the shock wave generated by a 45.5 kg HBX-1 charge detonated 10.1 m below the fluid-structure interface [17]. For all methods studied the simulation is run to a termination time of 150 ms and the time step is set at half the CFL limit.

Results

We begin by comparing the CAFE method (CASE with 1st order basis functions) and the CASE method with 8th order basis functions to Xiao's FE-FCT algorithm using a uniform mesh consisting of 81 total degrees of freedom (DOF). Comparisons to a benchmark CAFE obtained with a highly refined mesh in [17] showed that for 81 DOF the 8th order CASE method gives an adequate solution, thus we use it here as our basis of comparison. The benchmark solution taken from [17] is shown in Fig. 3 along with several other CASE solutions. Note that the solutions in Fig. 3 were obtained using the total field method, rather than the scattered field method. For both CAFE and CASE solutions the damping parameter, β [10], was set to 0.5. For Xiao's FE-FCT algorithm we set the diffusion and anti-diffusion coefficients, $\eta_D = \eta_A = 0.125$, and used the standard strong flux limiter (eq.(32)). For our modified double one-sided flux limiter (eq.(35)) we used diffusion and anti-diffusion coefficients, $\eta_D = 0.125$ and $\eta_A = 0.09$. All results were obtained using an in house FORTRAN 95 code.

Results for the vertical velocity of m_1 are shown in Fig.4a. For each method m_1 responds to the incident wave with a sharp rise in velocity to a peak or "kick-off" velocity of ~ 6.5 m/s. After this velocity is reached, the velocity begins to decay and take on a negative value as the cavitation region in the fluid grows. At 0.05 s the pressure wave generated by the closure of the cavitation region causes a second sharp rise in velocity. The reflection of the closure pulse back into the fluid causes a secondary cavitation region to form. After a rise to a second peak velocity the mass once again begins to fall into the fluid due to the presence of a second cavitation region. The second cavitation region is not as large as the first, occurring mainly in the fluid directly beneath the fluid [17]. Sprague and Geers [15, 37] refer to this phenomena as fluid accretion.

Figure 4a shows that m_1 is most susceptible to spurious pressure oscillations between 0.02s and 0.05 s. A close up view of the m_1 velocity response during this time frame is given in Fig. 4b. Comparing the various methods in Fig. 4b we see that while the CAFE solution does not exhibit any meaningful spurious oscillations it does not come close to matching the 8th order CASE solution. Based on the benchmark case shown in Fig.3, Xiao's FE-FCT method seems even more accurate than the 8th order CASE solution but suffers from very large spurious oscillations.

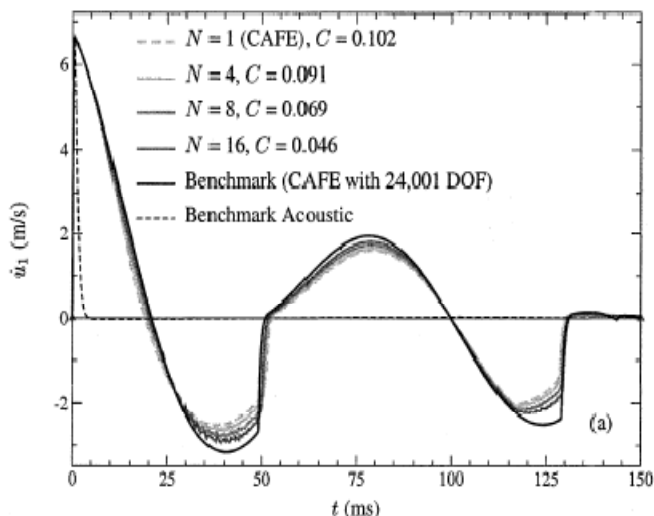
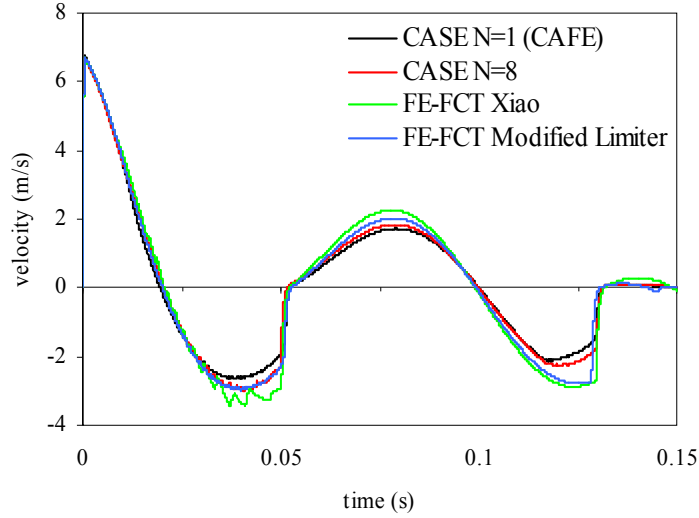
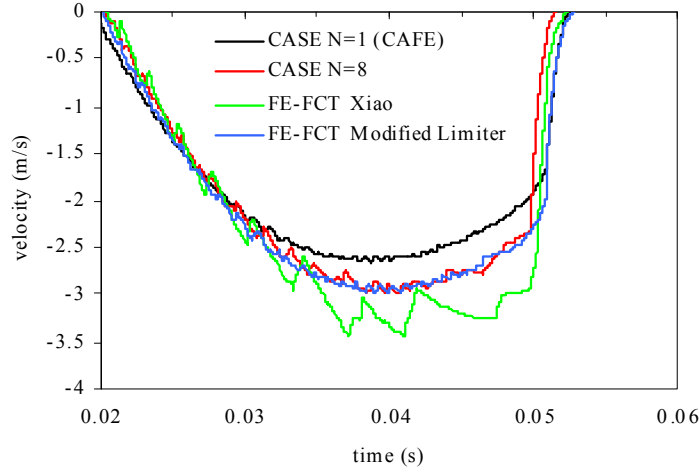


Figure 3. Benchmark solution and other 81 DOF CASE solutions for the mass-spring oscillator problem taken from [17]



(a)



(b)

Figure 4. 81 DOF FE-FCT solutions for \dot{m}_1 compared to 81 DOF CAFE and 8th order CASE solutions on two different time scales

In these oscillations we see the effects of the problems associated with applying the Xiao's FE-FCT scheme to the far-field UNDEX problem. The most significant of which is that the flux limiter cannot remove spurious oscillations unless the solution can be adequately smoothed during the diffusion stage. The result using Xiao's FE-FCT method also shows the rationale behind using the double one-sided flux limiter and over diffusing the solution. Figure 4b shows that the modified FE-FCT scheme is nearly identical to the 8th order CASE solution between 0.02 s and 0.05 s . Furthermore, the modified FE-FCT scheme does not suffer from the severe oscillations that the original method does. In fact we see a reduction in spurious oscillations when compared to the CASE solution.

Comparing results in Fig. 4a during the time period that the second cavitation region occurs (0.05 s – 0.13 s) both FE-FCT methods exhibit different results than the CAFE and CASE results. Both FE-FCT results show a much lower negative velocity and a sharper increase in velocity at the closure time of the second cavitation region. The reason for this difference in response occurs because the FE-FCT methods do not apply any damping or diffusion to the fluid-structure interface nodes. This hypothesis is supported by results in [39] which show a sharp rise in velocity at the closure time of the second cavitation region similar to that seen in the FE-FCT results. The results in [39] were obtained using the ghost fluid method instead of artificial damping. Because the second cavitation region is primarily fluid accretion, thus occurring at the fluid-structure interface or at the nodes immediately below the fluid-structure interface, any damping applied to the fluid-structure interface has an

exaggerated effect on the structural response. This exaggerated effect is seen for the CAFE and CASE results in Fig. 4a as the much more gradual velocity increase after the second cavitation region closes.

Based on the results of the 81 DOF test case, the modified FE-FCT method appears to offer the accuracy level of an 8th order CASE solution without the increase in spurious oscillations. The decrease in spurious oscillations is an advantage of the modified FE-FCT method, but the real advantage of the modified FE-FCT method lies in the reduction in computational expense. As we discussed previously, spectral elements produce larger maximum mesh eigenvalues and require smaller CFL when compared to linear finite elements. CASE offers a computational savings over CAFE only because the DOF required for an adequate CASE solution is less than that for a CAFE solution. Thus, by obtaining a CASE level of accuracy using linear finite elements with FE-FCT the computational savings increased even more. Figure 5 shows a comparison of CPU time required for a given number of fluids DOF. Figure 6 shows the of number of operations, taken as total DOF multiplied by the total number of time steps, required for a given number of fluid DOF. Comparing FE-FCT to the 8th order CASE in Figs. 5 and 6 shows that FE-FCT drastically reduces the computational expense for the 81 DOF test case. Note that in both Figs. 5 and 6 the CAFE method requires more operations and CPU time than FE-FCT because its CFL limit is slightly lower than for FE-FCT. This is due to its dependence on the amount of artificial damping used in the CAFE method.

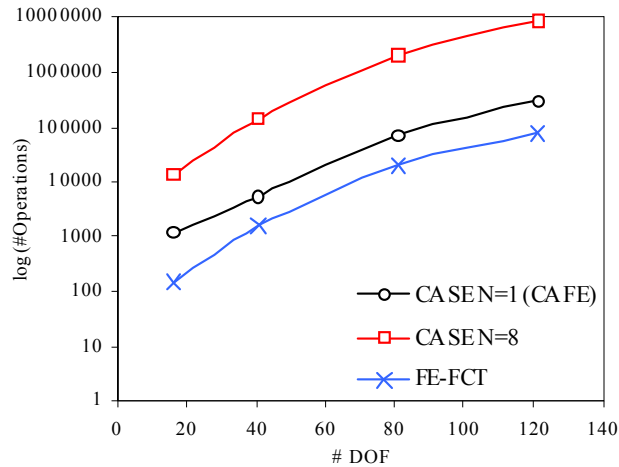


Figure 5. Number of operations (DOF x # Δt) required to run for a given number of DOF

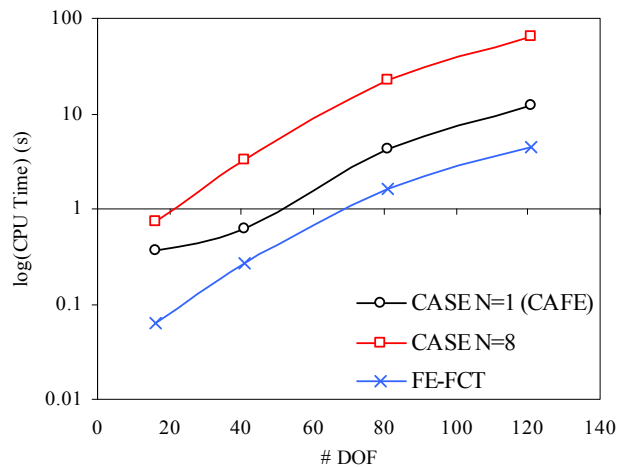


Figure 6. CPU time required to run for a given number of DOF

Conclusions

The capture of cavitation phenomena in numerical models of far-field UNDEX can be improved by applying the CASE methodology at the cost of increasing spurious oscillations in the problem domain. The FE-FCT method developed by Xiao used with a double one-sided flux limiter is effective in reducing the spurious oscillations associated with the CASE method and maintaining the improved cavitation capture. Furthermore, capture of small cavitation regions occurring in close proximity to the fluid-structure boundary may be improved by using FE-FCT because no artificial damping is applied on the fluid-structure boundary. Because the FE-FCT algorithm uses traditional linear finite elements rather than spectral elements to discretize the domain the FE-FCT algorithm results in a computational savings over CASE.

References

- [1] J. P. Boris, and Book, D.L., "Flux-Corrected Transport I. SHASTA, A fluid transport algorithm that works," *Journal of Computational Physics*, vol. 135, pp. 172-186, 1997.
- [2] Y. Shin, and Schneider, N., "Ship Shock Trial Simulation of USS Winston S. Churchill (DDG 81): Modeling and Simulation Strategy and Surrounding Fluid Volume Effects," in *74th Shock and Vibration Symposium*, 2003.
- [3] C. A. Felippa, and DeRuntz, J.A., "Acoustic fluid volume modeling by the displacement potential formulation, with emphasis on the wedge element," *Computers & Structures*, vol. 41, pp. 669-686, 1991.
- [4] O. C. Zienkiewicz, and Bettess, P., "Fluid-Structure Dynamic Interaction and Wave Forces. An Introduction to Numerical Treatment," *International Journal for Numerical Methods in Engineering*, vol. 13, pp. 1-16, 1978.
- [5] R. E. Newton, "Effects of Cavitation on Underwater Shock Loading - Part I," Naval Post Graduate School, Monterey, CA 1978.
- [6] R. E. Newton, "Finite Element Analysis of Shock-Induced Cavitation," in *ASCE Spring Convention* Portland, OR, 1980.
- [7] T. G. Liu, et.al., "Isentropic one-fluid modelling of unsteady cavitating flow," *Journal of Computational Physics*, vol. 201, pp. 80-108, 2004.
- [8] W. F. Xie, et.al., "Application of a one-fluid model for large scale homogeneous unsteady cavitation: The modified Schmidt model," *Computers & Fluids*, vol. 35, pp. 1177-1192, 2006.
- [9] O. C. Zienkiewicz, Paul, D.K., and Hinton, E., "Cavitation in Fluid-Structure Response (With Particular Reference to Dams Under Earthquake Loading)," *Earthquake Engineering and Structural Dynamics*, vol. 11, pp. 463-481, 1983.
- [10] C. A. Felippa, and DeRuntz, J.A., "Finite element analysis of shock induced hull cavitation," *Computer Methods in Applied Mechanics and Engineering*, vol. 44, pp. 297-337, 1984.
- [11] S. W. Gong, and Lam, K.Y., "On attenuation of floating structure response to underwater shock," *International Journal of Impact Engineering*, vol. 32, pp. 1857-1877, 2006.
- [12] C. F. Hung, Hsu, P.Y., and Hwang-Fuu, J.J., "Elastic shock response of an air-backed plate to underwater explosion," *International Journal of Impact Engineering*, vol. 35, pp. 151-168, 2005.
- [13] Y. S. Shin, "Total Ship Shock Modeling and Simulation Using LS-DYNA/USA," in *LS-DYNA User Conference 2000* Osaka, Japan, 2000.
- [14] S. L. Wood, "Cavitation Effects on a Ship-Like Box Structure Subjected to an Underwater Explosion." vol. Master of Science Monterey, CA: Naval Postgraduate School, 1996.
- [15] M. A. Sprague, and Geers, T.L., "A spectral-element/finite-element analysis of a ship-like structure subjected to an underwater explosion," *Computer Methods in Applied Mechanics and Engineering*, vol. 195, pp. 2149-2167, 2006.
- [16] M. A. Sprague, and Geers, T.L., "A Spectral-Element Method for Modeling Cavitation in Transient Fluid-Structure Interaction," *International Journal for Numerical Methods in Engineering*, vol. 60, 2004.
- [17] M. A. Sprague, and Geers, T.L., "A Spectral-Element Method for Modeling Cavitation in Transient Fluid-Structure Interaction," *Journal of Computational Physics*, vol. 32, pp. 1857-1877, 2003.
- [18] C. Pozrikidis, *Introduction to Finite and Spectral Element Methods using MATLAB*: Chapman & Hall/CRC, 2005.
- [19] C. Farhat, Lesoinne, M., and LeTallec, P., "Load and motion transfer algorithms for fluid/structure interaction problems with non-matching discrete interfaces: momentum and energy conservation, optimal discretization, and application to aeroelasticity," *Computer Methods in Applied Mechanics and Engineering*, vol. 157, pp. 95-114, 1998.

- [20] J. Giannakouros, and Karniadakis, G.E.M., "Spectral Element-FCT method for scalar hyperbolic conservation laws," *International Journal for Numerical Methods in Fluids*, vol. 14, pp. 707-727, 1992.
- [21] W. A. Mulder, "Spurious modes in finite-element discretizations of the wave equation may not be all that bad," *Applied Numerical Mathematics*, vol. 30, pp. 425-445, 1999.
- [22] J. Giannakouros, and Karniadakis, G.E.M., "A spectral element-FCT method for the compressible Euler equations," *Journal of Computational Physics*, vol. 115, pp. 65-85, 1994.
- [23] S. Xiao, "An FE-FCT method with implicit functions for the study of shock wave propagation in solids," *Wave Motion*, vol. 40, pp. 263-276, 2004.
- [24] D. L. Book, Boris, J.P., and Hain, K., "Flux-Corrected Transport II: Generalizations of the Method," *Journal of Computational Physics*, vol. 18, pp. 248-283, 1975.
- [25] J. P. Boris, and Book, D.L., "Flux-Corrected Transport. III. Minimal-Error FCT Algorithms," *Journal of Computational Physics*, vol. 20, pp. 397-431, 1976.
- [26] S. T. Zalesak, "Fully Multidimensional Flux-Corrected Transport Algorithms for Fluids," *Journal of Computational Physics*, vol. 31, pp. 335-362, 1979.
- [27] S. T. Zalesak, "The Design of Flux-Corrected Transport (FCT) Algorithms For Structured Grids," in *Flux-Corrected Transport: Principles, Algorithms, and Applications*, D. Kuzmin, Lohner, R., and Turek, S., Ed.: Springer, 2005, pp. 29-78.
- [28] G. E. Georghiou, Morrow, R., and Metaxas, A.C., "A two-dimensional, finite-element, flux-corrected transport algorithm for the solution of gas discharge problems," *Journal of Physics D*, vol. 33, pp. 2453-2466, 2000.
- [29] R. Lohner, Morgan, K., Peraire, J., and Vahdati, M., "Finite element flux-corrected transport (FEM-FCT) for the Euler and Navier-Stokes equations," *International Journal for Numerical Methods in Fluids*, vol. 7, pp. 103-109, 1987.
- [30] L. E. Kinsler, et. al., *Fundamentals of Acoustics - Fourth Edition*, 4th ed.: Wiley, 2000.
- [31] P. B. R. Nimmagadda, and Cipolla, J., "A pressure based cavitation model for underwater shock problems," in *71st Shock and Vibration Symposium*, Destin, FL, 2001.
- [32] ABAQUS, *ABAQUS v. 6.7 Users Manual*, 2007.
- [33] D. Givoli, *Numerical Methods for Problems in Infinite Domains*: Elsevier, 1992.
- [34] B. Klenow, and Brown, A., "Assessment of Non-Reflecting Boundary Conditions for Application in Far-Field UNDEX Finite Element Models," in *77th Shock and Vibration Symposium* Monterey, CA: SAVIAC, 2006.
- [35] J. A. DeRuntz, "Application of the USA Code to Underwater Shock Problems," in *73rd Shock and Vibration Symposium*, 2002.
- [36] D. L. Book, "The Conception, Gestation, Birth, and Infancy of FCT," in *Flux-Corrected Transport: Principles, Algorithms, and Applications*, D. Kuzmin, Lohner, R., and Turek, S., Ed.: Springer, 2005, pp. 5-28.
- [37] M. A. Sprague, and Geers, T.L., "Computational treatment of cavitation effects in near-free-surface underwater shock analysis," *Shock and Vibration*, vol. 8, pp. 105-122, 2001.
- [38] ABAQUS, *ABAQUS v. 6.7 Benchmarks Manual*, 2007.
- [39] W. F. Xie, et.al., "Dynamic response of deformable structures subjected to shock load and cavitation reload," *Computational Mechanics*, vol. 40, pp. 667-681, 2007.
- [40] R. H. Cole, *Underwater Explosions*: Princeton University Press, 1948.
- [41] M. Swisdak, "Explosion Effects and Properties: Part II. - Explosion Effects in Water," NSWC/WOR 1978.